Evidence for double resonant Raman decay from a Ag surface

F. O. Schumann* and Z. Wei†
Max-Planck-Institut für Mikrostrukturphysik, Weinberg 2, 06120 Halle, Germany

G. Di Filippo
CNISM and Dipartimento di Scienze, Universit Roma Tre, Via della Vasca Navale 84, 00146 Rome, Italy

G. Stefani
CNR-ISM, Via Fosso del Cavaliere 100, 00133 Roma, Italy

(Received 3 November 2022; revised 5 April 2024; accepted 6 June 2024; published 20 June 2024)

We have investigated the electron pair emission from a Ag(100) surface upon photon absorption which leads to the emission of a $4p$ photoelectron. The subsequent Auger decay proceeds in a single-step process as shown previously. Key finding was the emergence of a diagonal intensity feature in a two-dimensional kinetic energy distribution of the electron pair whose width reveals a characteristic time of 30 as for the dynamics of the core-hole decay process. We utilize this observation as a tool to identify an unexpected pathway of electron pair emission. Once the photon energy is at the threshold of a double $4p$ core hole creation we notice a sizeable broadening of the energy sharing distribution. We associate this process to the excitation of two $4p$ electrons between the Fermi and vacuum level followed by radiation less double electron excitation. This feature is characterized by an energy sum of the pair which disperses linearly with the photon energy. Therefore, we regard it as a double resonant Raman decay.

DOI: 10.1103/PhysRevB.109.245425

I. INTRODUCTION

Since the seminal work of Einstein on the photoelectric effect photoemission has evolved into an indispensable tool to characterize the electronic properties of matter. Angle-resolved energy distributions can be linked to the underlying band structure of the material in which an effective single-particle picture is commonly used. Enhanced energy and momentum resolution disclosed fine details of the photoemission spectra that are strictly related to many-body character of the system.

The very existence of the electron-electron interaction is responsible for the absorption of a single photon that leads to multielectron emission. A prominent example for two electrons is the emission of a photoelectron and a concomitant Auger electron. On this effect are based powerful tools for the chemical characterization of surfaces known as x-ray photoelectron spectroscopy (XPS) and Auger electron spectroscopy. Gas phase experiments have revealed additional channels leading to electron pair emission, e.g., double Auger decay [1–4]. The emission of three or four electrons upon single photon absorption is also well-documented [5,6]. Multiple electron emission events have experienced renewed interest with the availability of intense and ultrashort light pulses from synchrotron and laser sources. These allow to address fundamental questions on the time evolution of the electron dynamics on the attosecond (as) timescale [7–10].

If the photon energy approaches the threshold for a core level excitation, one can observe resonant photoemission. It leads to additional satellite peaks in the valence band photoelectron spectrum, e.g., Ni and Cu, whose explanation rests, in this specific case, on a picture of two correlated $3d$ holes [11–13]. These extra satellites are a manifestation of the electron correlation among the valence electrons.

Intimately related to resonant photoemission is the resonant Auger-Raman effect [14]. Near the threshold photon energy a core electron populates a state just above E_F but below the vacuum level. The sample is now in an autoionizing state and an Auger transition takes place. The exited core electron may or may not take part in this process leading to the so-called participator or spectator decay. Unlike in regular Auger decay, in which the kinetic energy is independent of the photon energy, the spectator decay does display a linear dispersion [14,15]. This is then referred to as resonant Raman decay, it can be utilized to determine the timescale of electron dynamics which is referred to as core-hole clock spectroscopy [16].

We will demonstrate that when the photon energy matches twice the binding energy of a core state, the conventional process of single core electron ionization followed by emission of a single Auger electron, can be accompanied by a

*Contact author: schumann@mpi-halle.de
†Present address: College of Materials Science and Engineering, Chongqing University, 400044 Chongqing, PR China.

competing two electrons resonant Raman process. The latter channel implies the promotion of a pair of core electrons to an excited bound state that eventually decays by filling up the two core holes and ejecting a pair of valence electrons that continuously share the excess energy. To prove the existence of such an excitation de-excitation process we have performed an Auger-photoelectron coincidence spectroscopy (APECS) investigation of the photon energy dependence of the electron pair emission from a Ag(100) surface. We find that the distribution of Auger-photoelectron pairs peaks along the lines of constant sum energy ($E_{\text{sum}} = E_{\text{photoelectron}} + E_{\text{Auger}}$) of the 2D energy plot and is well-approximated by a Lorentz line shape with FWHM of roughly 23 eV; see Appendix B. At 118 and 124 eV the energy sharing between E_{left} and E_{right} cannot be described by the sum of two Lorentzians approximately 20 eV wide as it was done at higher and lower photon energies. To justify the absence of a sharp local minimum at $E_{\text{diff}} = 0$, it is assumed to come from the contribution of a third Lorentzian centered at equal energy sharing. We regard this finding as evidence for a competing pathway for electron pair emission. We interpret this as a double core hole creation followed by relaxation via a double resonant Raman decay.

II. EXPERIMENT

We utilized a coincidence set-up with a pair hemispherical analyzers with 200 mm mean radius which we call "left" and "right," respectively [17–20]. The electron-optical axes of the two spectrometer are perpendicular to each other and define the x and y axis, see Fig. 1. Within this scattering plane the angular acceptance is $\pm$ 15°. The photon beam is perpendicular to the scattering plane and defines the z axis. The sample manipulator axis is within the x-z plane such that the incoming light has a grazing angle of 10° with the [010] direction of the Ag(100) surface. The surface normal has an angle of 45° with respect to the spectrometer aligned along the x axis [21]. They are equipped with channel plates with resistive anodes as position sensitive detectors to record the impact position. We employ a four-way coincidence circuit in which the channel-plate signals have to be within 165 ns while at the same time the electronics of the resistive anodes indicate a successful impact position determination. The latter are needed to determine the kinetic energy of the coincident particles. For each valid event the arrival time (t_{left} and t_{right}) at the respective detector with respect to the coincidence trigger is known. This allows to compute the arrival time histogram $dt = t_{\text{left}} - t_{\text{right}}$ and this will show a peak residing on a constant background. The emergence of a peak is evidence of "true" coincidences as discussed in the pioneering work of Bothe and Geiger and established in the literature [22–24]. Two independent photons can also lead to the emission of two uncorrelated electrons termed of "random" events. We adopted established procedures to remove this contribution, all spectra we present have been corrected in this way [17–20]. We will introduce an unexpected pathway of pair emission, therefore we want to be more specific on the details of this procedure as explained in Appendix A.

The measurements were performed with a pass energy of 300 eV and an entrance slit of 1 mm. The energy window which is dispersed onto the channel-plate detector amounts

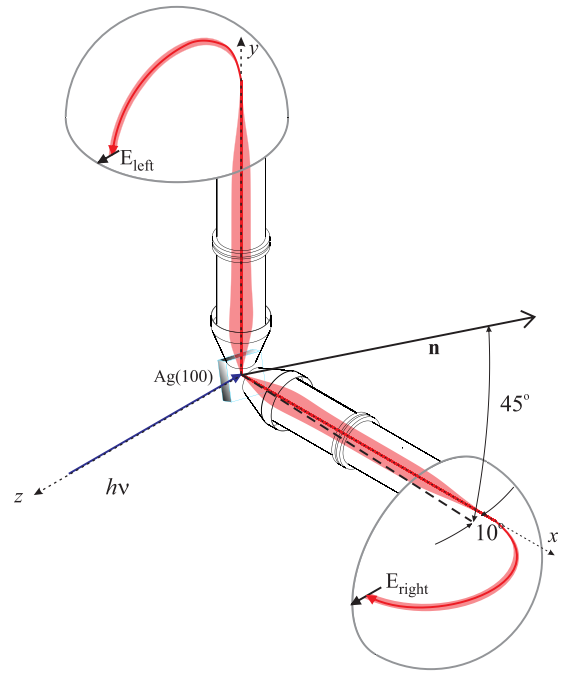

FIG. 1. Geometry of the experiment. The two spectrometer define a scattering plane and the electron-optical axes of the spectrometer are perpendicular to each other. They define the x and y axis. The propagation direction of the UV radiation is along the z axis. The manipulator axis is within the x-z plane tilted by an angle of 10°. The surface normal **n** of the sample encloses an angle of 45° with the x axis.

to 27 eV, while the resolution is 0.8 eV. In contrast to the usual operation of electron spectrometer we do not scan the energies, but fix the energy. All kinetic energies are referred to the vacuum level of the sample held at room temperature. The output of the experiment is efficiently represented by false color tridimensional plots of the coincidences count rate versus the kinetic energy E_{left} and E_{right}: in short the 2D-energy distributions. The preparation of the Ag(100) surface followed standard procedures of Ar^+ sputtering and annealing. The base pressure of the chamber was 5×10^{-11} mbar. We utilized the beam line UE56/2-PGM-2 of the BESSY-II electron storage of the HZB/Berlin [25,26]. We performed measurements with light of both circular polarization and present the polarization integrated spectra.

Each coincidence event with the associated information is stored in a list. This allows a post-experimental analysis. In this work we will show three different energy distributions obtained from this list. These are the 2D-energy presentations, the energy sum and sharing curves. The latter are obtained by an energy constraint on the sum energy as discussed later.

III. ENERGY SPECTRA

Usually it is assumed that the emission of an Auger electron proceeds through a sequential process after the core electron emission. This two-step evolution is a reasonable approximation whenever the core-hole lifetime is longer than the electron-electron interaction time and the core-hole relaxation does not affect the autoionizing Auger decay [27]. In

general, this is not the case and core ionization and Auger decay are intimately correlated in a one-step process [27]. The Coster-Kronig decay involving the $4p$ level for Ag and Pd and the $3p$ level of Cu are paradigmatic examples of such a correlated behavior that manifests itself in experiments with an extraordinary large line width of the core level spectra [19,28–31]. The underlying physics could be related with a rapid fluctuation of the intermediate state between two configurations. This is responsible for a breakdown of the single electron picture. The key signature is a diagonal intensity band within a 2D-energy distribution of the emitted electron pair that speaks for a strong covariance (correlation in energy) of the two final unbound electrons.

In Fig. 2 we present the 2D-energy distributions for the $4p$ NVV electron pair emission of Ag(100) as measured at three different photon energies. In each panel we have included a black diagonal line which presents the maximum energy sum $E_{\rm sum}^{\rm max}$ a pair can have. The entity is defined as the difference of the photon energy and twice the work function ϕ that is $E_{\rm sum}^{\rm max} = h\nu - 2\phi$. The work function for the Ag(100) surface is $\phi = 4.4$ eV. Common to all plots is an almost vanishing intensity near the $E_{\rm sum}^{\rm max}$ line. Upon moving away from this line the intensity starts to pick up and finally a high intensity region parallel to the $E_{\rm sum}^{\rm max}$ line emerges. Its energetic position is the same with respect to the $E_{\rm sum}^{\rm max}$ line for all photon energies. We have highlighted this by adding a pair of dashed diagonal lines in the energy presentations. These have all the same energy position with respect to the $E_{\rm sum}^{\rm max}$ line. The emergence of the diagonal intensity ridge demonstrates that the formulation of a two-step process for the $4p$ Auger decay is incorrect [28]. The diagonal intensity ridge has the largest (along the constant $E_{\rm sum}$ diagonal) extension for $h\nu = 118$ eV, while for the other two photon energies it is much narrower, roughly 20 eV in both cases. For the experiments plotted in Figs. 2(a) and 2(b) both spectrometer covered the same energy window, while for the measurement in Fig. 2(c) the settings where very different. In the latter case the intensity maximum is at the energy coordinate 38 eV/142 eV. From symmetry considerations there must exist an additional intensity maximum at 142 eV/38 eV, which we can only see if the spectrometer settings are exchanged. In other words the full energy spectrum consists of two intensity maxima along a diagonal line, see Appendix B. While the 2D-energy spectra display a strong photon energy dependence this is not the case for the sum energy spectra shown in Fig. 3. In this figure we employ as x axis the two-particle binding energy E_{2e}^{B}, which measures the energy sum of the emitted pair with respect to the $E_{\rm sum}^{\rm max}$ value, i.e., the binding energy of the final two-hole state $E_{2e}^{B} = h\nu - E_{\rm sum}$. The spectra are very similar in shape and energetic position despite the large variations of the diagonal intensity feature in Fig. 2. The intensity maximum is at 16.7–17.0 eV and a shoulder is visible around 10 eV. Toward higher-binding energy values the intensity decreases almost linearly. This decrease is a consequence of the decreasing number of energy channels at the lower left-hand corner of the 2D-energy plots in Fig. 2.

If the Auger process leads to two vacancies in the valence band, then the simplest description of the Auger line shape is a self-convolution of the valence band single particle density-of-states (DOS) [32]. A more sophistic treatment uses this as input together with the electron-electron interaction described by a parameter $U_{\rm eff}$ [33,34].

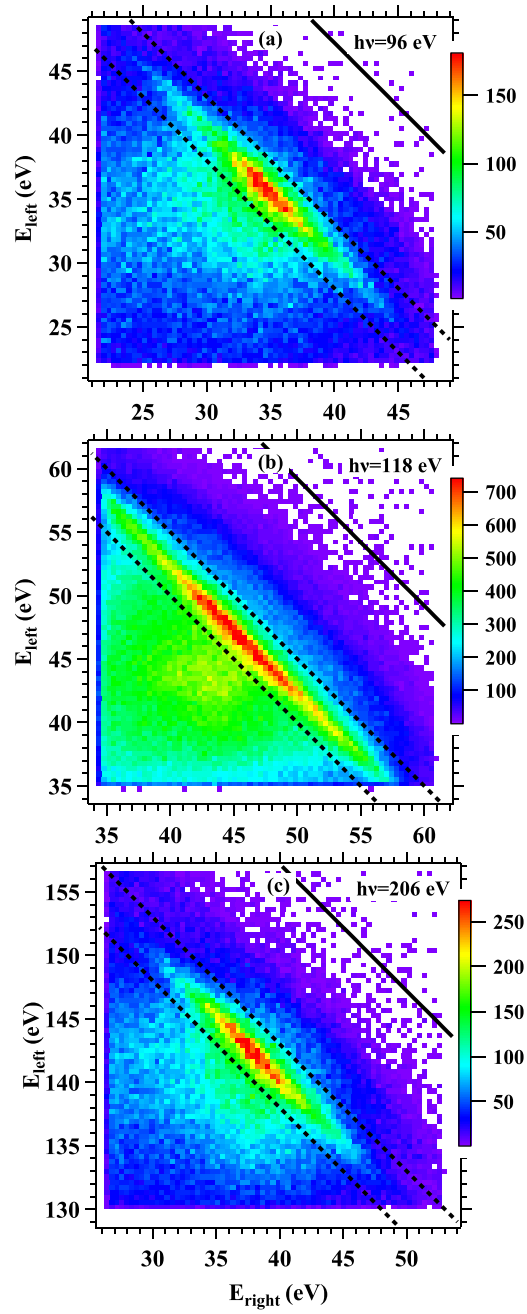

FIG. 2. Photon energy dependent 2D-energy spectra. In panels (a) and (b) both spectrometer cover the same energy window. In panel (c) different energy windows are selected. The solid diagonal lines refer to the position of $E_{\rm sum}^{\rm max}$. The pairs of dashed lines indicate the energetic region used for the sharing curves. They are 16.7 ± 2.5 eV below $E_{\rm sum}^{\rm max}$.

The DOS of the Ag valence band is high for binding energies centered at 5 ± 2eV below E_F where 10 $4d$ electrons are located. The strongly dispersing $5sp$ band, from about 8 eV below up to E_F, contributes with one electron. Therefore, the probability to remove two electrons from E_F is strongly reduced compared to the $4d$ band region. The valence band spectrum measured with XPS can be regarded as

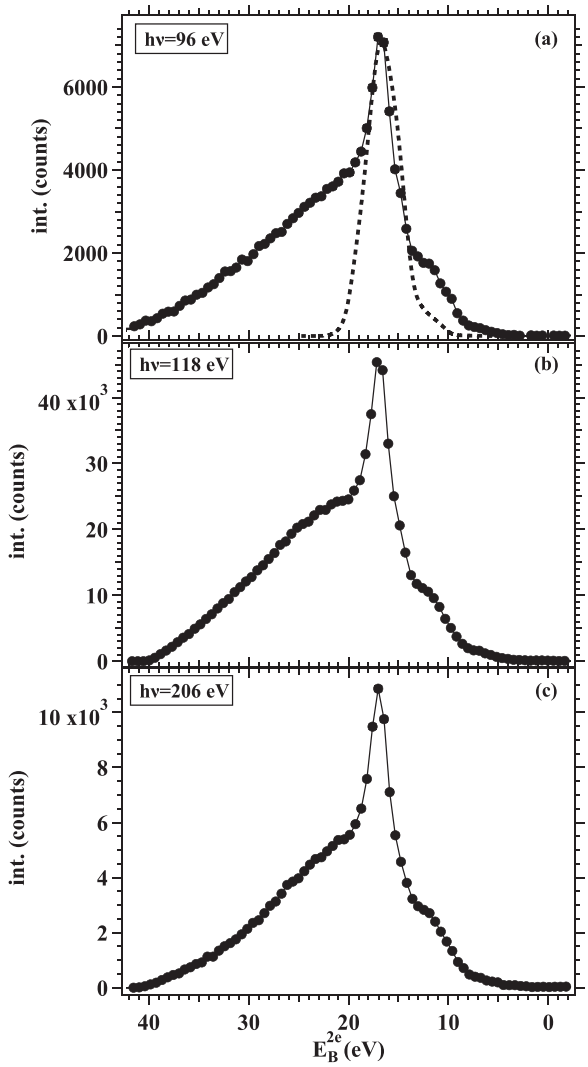

FIG. 3. We show the E_{sum} spectra measured at different photon energies. The coincidence rate was integrated along constant E_{sum} lines of Fig. 2. In panel (a) we have included the self-convolution of the valence band DOS shifted by 5.6 eV (dashed curve).

a good approximation of the single particle DOS. Therefore, we used published data from a Ag surface as the input for the self-convolution which has been included in Fig. 3(a) as dashed curve [35]. To account for the electron correlation in a simple manner we shifted this curve by 5.6 eV toward higher two-hole state binding energies. This energy shift is in line with more detailed investigations of the Auger line shape in single electron spectroscopy and APECS measurements [36,37]. The intensity peak at $E_B^{2e} = 16.7$ eV is therefore due to contributions which leave two vacancies in the $4d$ valence band. In our previous work we have associated this with $4d^{-2}$ multiplets [28]. The low intensity near $E_B^{2e} = 0$ is a consequence of the low occupancy of the strongly dispersing $5sp$ band.

At this point we emphasize that the description of the $4p$ hole state in terms of a spin-orbit doublet is questionable. This due to the breakdown of the single electron picture in the case of the Ag $4p$ as discussed earlier [28,31]. The rapid fluctuation between different short lived intermediate ionic configurations is the strong energy covariance of the two final unbound electrons, see Fig. 2.

TABLE I. Experimental ionization energies of single I_p^+ and double core hole creation I_p^{2+} on the $1s$ levels C, N, and O [3,6,48–50]. The term R^I_{exp} is the ratio of the experimental double and single ionization energy. The prediction from Slater [47] is given by R^I_{mod}.

1s Orbital	I_p^+(eV)	I_p^{2+}(eV)	R^I_{exp}	R^I_{mod}
C in CO K^{-2}	296.2	666.7	2.25	2.25
C in C_2h_6 K^{-2}	290.6	650.6	2.24	2.25
C in CH_4 K^{-2}	290.8	651.5	2.24	2.25
N in N_2 K^{-2}	409.9	902.5	2.20	2.20
N in NH_3 K^{-2}	405.6	892.0	2.20	2.20
O in O_2 K^{-2}	543.1	1179.2	2.17	2.17

IV. LINE SHAPE ANALYSIS

After the first qualitative description of the intensity band in Fig. 2 we proceed in a more quantitative way. For this we discuss the line shape of the diagonal intensity band. We choose those events which possess a sum energy centered at the peak position of the curves shown in Fig. 3. This window is characterized by $E^B_{2e} = 16.7 \pm 2.5$ eV visualized by the dashed lines in Fig. 2. The energy width encompasses the full span of the final two hole multiplet structure and furthermore ensures sufficiently low statistical uncertainty.

The sharing curves in Fig. 4 are obtained with four different photon energies. In such a presentation the intensity is plotted against the energy difference $E_{\text{left}} - E_{\text{right}}$. Hence, they represent the probability distribution for sharing of the energy between the two final electrons. In Figs. 4(a) and 4(b) we show the data for $h\nu = 96$ and 206 eV, respectively. At these photon energies the extension of the diagonal feature is the smallest and identical, as it should be determined by the intermediate state lifetime, see Appendix B. The energy sharing curve for $h\nu = 96$ eV has a peak at $E_{\text{left}} - E_{\text{right}} = 0$ eV. In this sense Auger and photo electron have the same kinetic energy. As stated above the theoretical description of the broad $4p$ line width of Ag incorporated a rapid fluctuation of the intermediate state, hence a rather short lifetime that implies a natural line width larger than the experimental resolution. This motivates to attempt a description of the sharing curve via a Lorentz curve. The red curve is a Lorentzian fit to the data and the agreement is rather good as evidenced by the residual shown on top of the plot. We find a full width at half maximum (FWHM) of 20 eV $\pm$ 0.5 eV for $h\nu = 96$ eV. The energy window for the analysis is given by the energy range covered by the red curve. Essentially we use all events except for those near the edge of the detection window. An equivalent analysis was done for the $h\nu = 206$ eV data. Again a Lorentzian line shape is a good description and the FWHM is slightly larger with 23 $\pm$ 0.6 eV. The peak position is now at a large energy difference of 104 eV, because of the increase in the photon energy. While the Auger electron energy is unaffected by the photon energy, the photo electron will linearly disperse with the photon energy. The energetic position of the Auger electron is in agreement with positron stimulated Auger

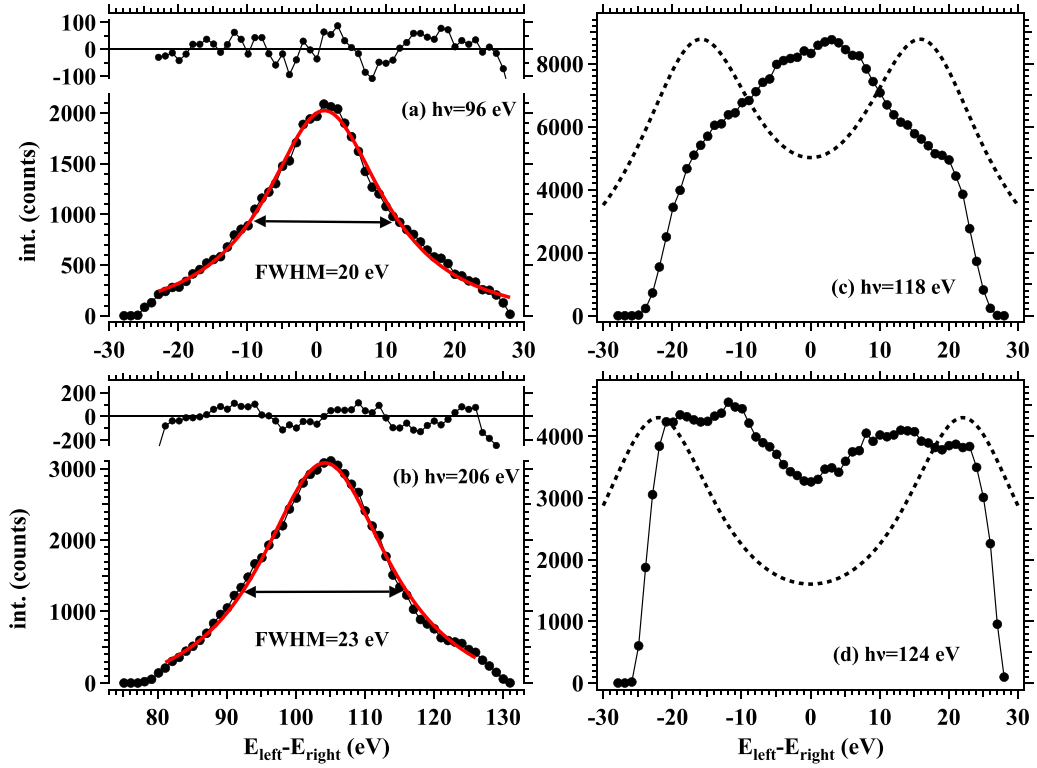

FIG. 4. Panels (a) and (b) show the sharing curve obtained with $h\nu = 96$ and 206 eV, respectively. We fixed the two-particle binding energy to $E^B_{2e} = 16.7 \pm 2.5$ eV. The line shape was fitted to a Lorentzian (red curve). The residual is seen at the top of each panel. Panels (c) and (d) show the sharing curves for $h\nu = 118$ and 124 eV. The dashed curve is a simulation of two Lorentzian curves, see text.

emission due to $4p$ core electron annihilation from a Ag(100) surface [38].

If our spectrometer were able to cover a larger energy range, we would have detected a second peak in the sharing curve centered at an energy difference of −104 eV. The applicability of a Lorentz curve is relevant on two accounts. First, it establishes that the width of the sharing curve (for constant energy sum) is a consequence of the lifetime of the core hole intermediate state in the Auger decay. From the width we deduce a characteristic time of 30 as. Second, any deviation from a Lorentz curve we associate with a deviation from a single pathway electron pair emission.

Therefore, we want to adopt a simulation of the sharing curve based on a Lorentzian line shape with an equal FWHM. More precisely it consists of two Lorentzian curves whose peak positions depend on the photon energy. The result of the simulation for photon energies identical to the experiment is shown in Figs. 4(c) and 4(d). If the photon energy is $h\nu = 118$ eV, then we expect the peaks of the sharing curves at ± 16 eV, which increases to ± 22 eV for $h\nu = 124$ eV. These simulated curves have been added as dashed curves to the experimental data presented in Figs. 4(c) and 4(d). In both instances we expect a well-developed minima for equal energy sharing. Near the boundary of the energy window we should expect maxima. However, this is in contrast with the experimental data. There is still a maximum at equal energy sharing for $h\nu = 118$ eV which evolves to a local minimum for a slightly larger photon energy of $h\nu = 124$ eV.

A line shape analysis for those two photon energies is reliable only in the range $E_{\text{left}} - E_{\text{right}} \cong \pm 15$ eV. Within this interval the coincidence detection efficiency is constant. Outside this energy window, we have reached the edge of the channel-plate detector and the detection efficiency quickly drops to 0 for $E_{\text{left}} - E_{\text{right}} \cong \pm 27$ eV.

The operation with unequal spectrometer settings for $h\nu = 124$ eV allows to access a different range of energy sharing, namely the interval $E_{\text{left}} - E_{\text{right}} = -8$ to +44 eV with an almost constant efficiency in the reduced range +8 to +33 eV only. This has been done and Fig. 5 reveals a peak of the sharing curve at 22 eV. This is the expected position from our simulation, see dashed curve in Fig. 4(d). Not only the peak position is as expected, but also a Lorentz line shape with a FWHM of 22 eV is a good approximation.

We should point out an inconsistency in the data of Figs. 4(d) and 5. For the latter we find that the ratio of the peak intensity to the equal sharing values is about 4.8. Such a deep minimum is not present in Fig. 4(d). In this case the intensity ratio is around 1.3. This discrepancy can be explained by an unusual behavior of the detection efficiency. In the preparation of these measurements at the synchrotron and between measurement shifts we have performed electron pair emission studies [termed (e,2e)] by means of a primary electron beam. The emission of the $4d$ valence band leads to the emergence of diagonal intensity band with roughly constant intensity [39]. By adjusting the primary energy, but keeping the spectrometer settings fixed, one can move the detected energy range. In the case of the unequal energy settings utilized for Fig. 5 the (e,

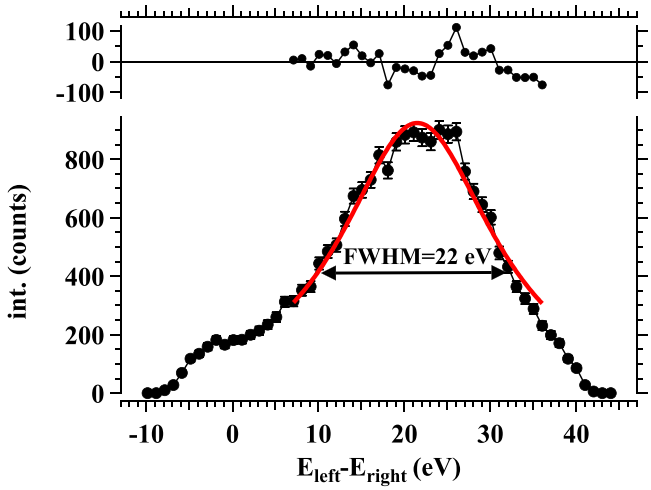

FIG. 5. Sharing curve obtained with $h\nu = 124$ eV. We fixed the two-particle binding energy to $E^B_{2e} = 16.7 \pm 2.5$ eV. The line shape was fitted to a Lorentzian (red curve). The residual is seen at the top of the panel.

2e) measurement revealed an almost constant sharing intensity within the peak region. Toward more negative sharing the intensity drops and for equal sharing it is roughly a factor 2.5 smaller than in the region of constant intensity.

The main observation is an emergence of an electron pair emission channel which is not due to the Auger decay following a single $4p$ core level excitation. It shows up if the photon energy is in the range of 118–124 eV.

One may consider the participation of the $4s$ level as the origin of the extra pathway. The binding energy of the $4s$ level is 98 eV, hence the core resonant DPE process related to this level is possible at $h\nu = 118$ and 124 eV. For $h\nu = 118$ eV the photoelectron has an energy of 15.4 eV, which is outside the detection window, see Fig. 2(b). Hence, the $4s$ related Auger decay does not play a role.

So far we have discussed the core-resonant process, but it is also possible that two valence electron are being emitted without the participation of a core-electron. This process is known as double photoemission (DPE). Experiments on a Ag(100) surface with photon energies up to 60 eV have shown that the intensity is in an energy window consistent with the 2e-DOS [40,41]. Specifically, there is no need to introduce an energy shift for the 2e-DOS as done in Fig. 3(a). This speaks against a contribution of the DPE pathway in the sharing curves with the effect of additional intensity at the position of the minima of the simulation (at equal energy sharing).

V. ALTERNATIVE PATHWAY OF ELECTRON EMISSION

We want to introduce a pathway which can account for the intensity at equal energy sharing observed in Figs. 4(c) and 4(d). Due to the fact that additional intensity is along a diagonal line in the 2D-energy spectrum we need to assume a single-step process. Further, the sum energy of this path has the same two-particle binding energy, see Fig. 3. This means that the final state must be the same, namely a double vacancy in the $4d$ band. This condition is fulfilled in the cartoon presented in Fig. 6(a). A photon lifts an electron pair

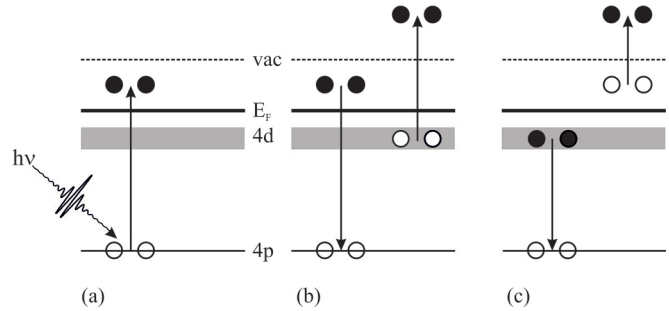

FIG. 6. Cartoon of double core hole creation (a) and subsequent double Auger emission via two pathways (b) and (c).

from the $4p$ level above the Fermi level, but below the vacuum level. This means that the photon absorption does not lead to photoelectron emission. The absorption of a single photon by an electron pair is certainly possible as it is the essence of double photoemission. The sample is now in an autoionizing state and can relax via filling of the double $4p$ vacancy and subsequent electron pair emission. For this process one can imagine two scenarios. In Fig. 6(b) the excited electron pair returns to the $4p$ level and is followed by an electron pair emission from the $4d$ level. Conversely, in Fig. 6(c) it is an electron pair from the $4d$ level that transfers its energy to the electron pair residing above E_F. Both pathways will lead to a double vacancy in the $4d$ valence band, while an electron pair is emitted.

Our model incorporates observed outcomes in electron coincidence spectroscopy which we recall briefly. One is the effect of double Auger decay. Upon filling a single core vacancy the energy gain can be transferred to two electrons [42–44]. In C and N-ion collisions with Ni surfaces and carbon foils it was discovered that the electron emission spectrum also contained intensity at twice the nominal Auger electron energy of the projectile [45,46]. This was explained by a three-electron Auger decay in which a double vacancy is filled by an electron pair and the resulting energy is transferred to a single electron. Hence, our proposed scheme is a combination of these two effects.

A consequence of the proposed scenario is that it is active only in a narrow photon energy range which needs to be specified. The energetics are summarized in Table I. In a first step we want to explore the description by Slater [47]. There the total energy of an atom is determined by a sum of hydrogenic energy terms of the orbitals with appropriate shielding constants and main quantum number. To derive an ionization/excitation energy the total energy of this changed orbital occupation is determined. The energy difference to the atomic value is then the ionization/excitation energy. To validate this procedure we have applied it to published data on double core hole (DCH) creation on molecules using as input the single core hole excitation data [3,6,48–50]. The DCH studies concerned the creation of double holes in the $1s$ levels of C, O, and N. The holes are on the same site (K^{-2}). The reported double ionization energy (I_p^{2+}) is divided by the single ionization energy (I_p^{+}) leading to the column $R^I_{\rm exp}$. The last column $R^I_{\rm mod}$ is obtained using Slater's work [47]. Despite the simplicity of Slater's description the calculated

values are not dissimilar from the experimental ones. This motivates us to utilize it for our scenario. We point out that Slater treats s and p levels as one group. Hence, we will change the occupation of the a $4sp$ level and not the $4p$ level. With this in mind we determine the energy for the creation of an Ag^+ ion with a $4sp^{-1}$ hole. Likewise we determine the energy necessary to create an excited Ag atom with two $4sp$ vacancies in which the two $4sp$ excited electrons occupy the $5s$p level. The ratio of the double excitation energy to the single ionization energy is then 1.97.

A more accurate account would be a Hartree-Fock calculation of the Ag atom/ion in which the $4p$ level occupancy is changed. This has been done via a commercial software [51]. This leads to an energy ratio of double excitation versus single ionization of 1.98. From this we conclude that the minimum photon energy for double core excitation would be roughly twice the binding energy of the $4p$ level. If we use the value for the least bound part we obtain 114 eV. If one increases this by twice the work function we obtain 122.8 eV, at this photon energy at least one of the excited $4p$ electrons is emitted and not available for the suggested scenario. For more tightly bound $4p$ electrons the required photon energy will be higher. This means the suggested scenario is possible on the basis of energy considerations. Due to the fact that energy sum of the pathway moves with the photon energy we have a two-electron extension of the resonant Auger-Raman effect [14,16]. At first sight these combinations of processes appear a rather unlikely outcome. While the autoionizing part is expected to occur with high probability the promotion of two $4p$ electrons with a single photon just above E_F is less likely. However, the pathway takes place at photon energies near the Cooper minimum for photoemission, thus making it easier to reveal second-rank effects [52,53].

VI. SUMMARY

We have investigated the electron pair emission from a Ag(100) surface upon photon absorption. Apart from the conventional Auger decay due to a single $4p$ core hole creation, we identify an unexpected pathway for double electron emission. It appears for photon energies near the threshold for $4p$ double core hole creation. To identify the nature of this decay channel we make use of the fact that the conventional Auger decay possesses a characteristic spectroscopic signature which is a Lorentz line shape of the energy sharing. Therefore the sharing curve is dominated by the intermediate state lifetime broadening and we infer a timescale of 30 as for the correlated electron dynamics of the conventional Auger decay. To explain the anomalous not-Lorentzian energy sharing distribution observed for photons close to the $4p$ double excitation threshold, we propose a microscopic picture in which the two excited $4p$ electrons reside between E_F and the vacuum level. The subsequent relaxation leads to the emission of an electron pair. The spectroscopic weight of this pathway moves with the photon energy, hence we term it as double resonant Raman process.

ACKNOWLEDGMENTS

We thank the HZB for the allocation of beamtime and W. Mahler and B. Zada for the user support. We acknowledge J. Kirschner for his support and fruitful discussions. A. Zacarias helped us to set up the Hartee-Fock calculations.

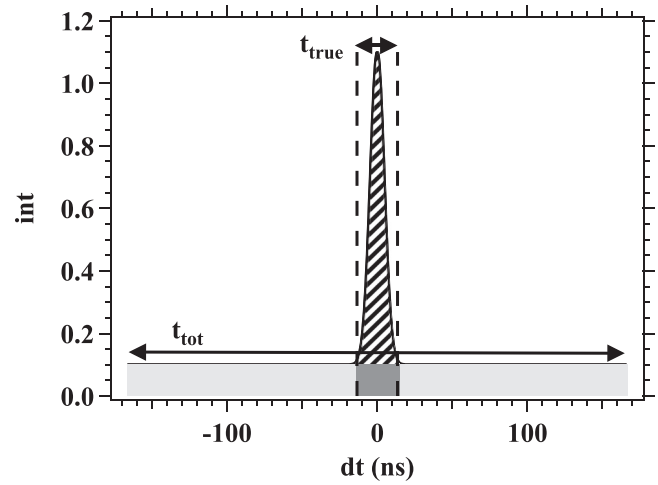

FIG. 7. Schematic arrival time histogram of total width t_{tot}. A Gauss fit gives a region of interest with width t_{true} as indicated by the pair of vertical dashed lines. The number of "true" events is determined by the hatched area. The light-gray area represents the number of "random" events outside the peak region. The dark-gray area is a measure of the "random" events in the region of interest.

APPENDIX A: RANDOM BACKGROUND REMOVAL

In view of the fact that the new process envisaged is a second-rank one, we consider it useful to discuss the accuracy with which the discrimination of the "true" from the "random" coincidences is carried out in the experiment. We have described details of our coincidence spectrometer in previous work [17–19,41]. We want to recall important points on how to deal with the unwanted intensity due to "random" events. The "random" events have their origin in the emission of uncorrelated electrons due to two independent photons. The rate of those events scale quadratic with the primary flux while the "true" events go linear with the flux and to achieve a large "true" versus "random" ratio (TR-ratio) one has to reduce the flux significantly. This is a general experimental difficulty and it is generally accepted that the TR-ratio should be kept above 1. There is a straightforward way to determine this ratio with our instrument which we discuss via Fig. 7 [17,41].

We display the arrival time difference dt curve. This is given by the flight time difference of two electrons reaching the respective detectors. The total width of the dt curve is given by t_{tot}, this was electronically set to 330 ns. We determine the temporal width t_{true} which incorporates "true" coincidences in the following way. There is no time correlation between two incoming photons which are absorbed by the sample. Consequently there is no preferred time difference in the flight times of these two electrons. This leads to a continuous intensity level for "random" counts. This is different from the emission of two electrons constituting "true" events. This

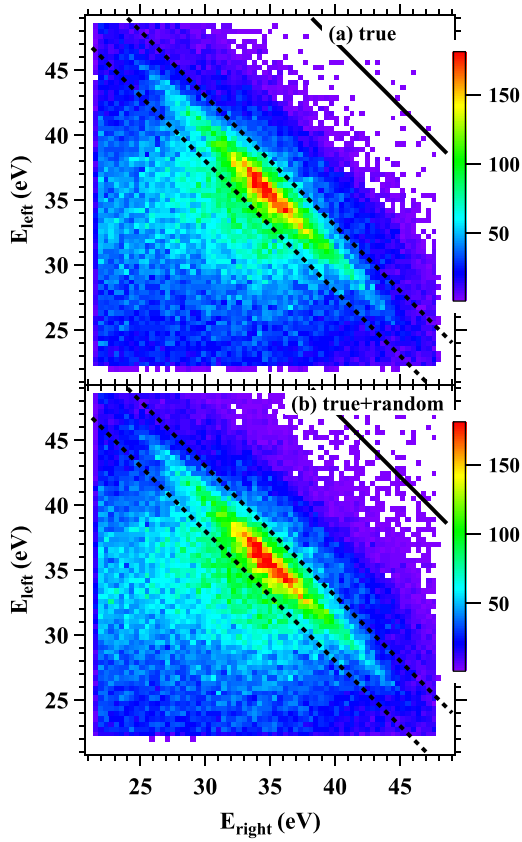

FIG. 8. 2D-energy distributions for $h\nu = 96$ eV. In panel (a) we plot the "true" counts while panel (b) presents the "true" and "random" counts. The solid diagonal lines refer to the position of $E_{\text{sum}}^{\text{max}}$. The pairs of dashed lines indicate the energetic region used for the sharing curves in the main text.

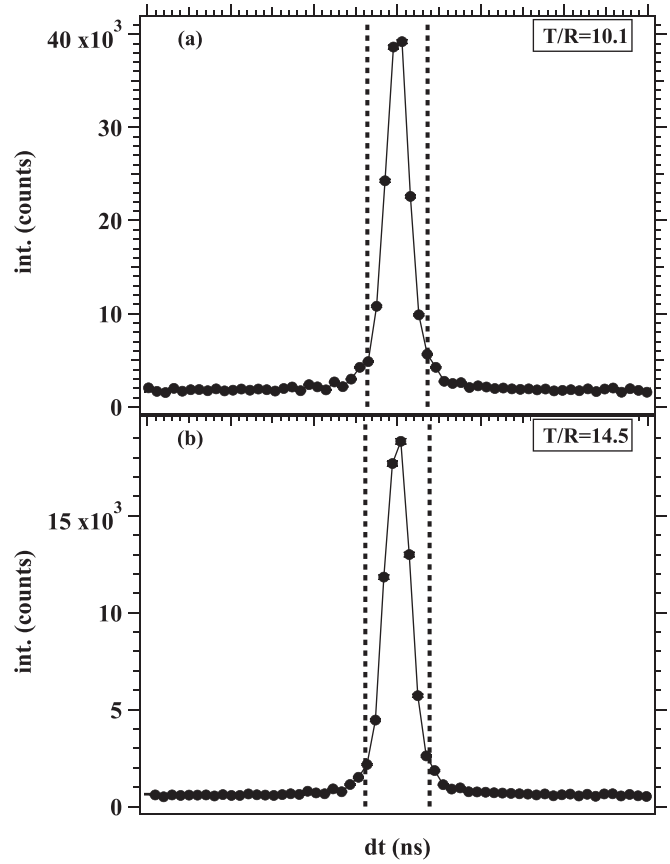

FIG. 9. Evaluation of the dt histogram for the measurement with $h\nu = 96$ eV. In panel (a) all data leading to the 2D-energy distribution in Fig. 8 are shown. Panel (b) is result for the subset bounded by the dashed diagonal line in Fig. 8.

occurs, within the experimental time resolution, at the same time leading to a peak in the dt spectrum.

With this reasoning we perform a fit with a Gaussian curve (see Fig. 7), which defines a region of interest where "true" coincidences are located. For this we take twice the FWHM multiplied by 1.05 this gives the value of t_{true}. This is a good description of the base width of the peak indicated by the pair of vertical dashed lines; see Fig. 7 [41]. The peak width is in accordance with the time dispersion of the spectrometer [54,55]. A typical value for the FWHM is 7 ns for a pass energy of 300 eV and 1 mm slit size. For each coincidence event we determine whether it falls within the region of interest centered around the peak of the histogram. This leads to two energy distributions, in one we have "true" and "random" counts, while the other has only "random" events. The window which includes only "random" counts has a width of $t_{\text{tot}} - t_{\text{true}}$. This we scale by a factor $t_{\text{true}}/(t_{\text{tot}} - t_{\text{true}})$. If we take now the difference, then we have effectively a spectrum of "true" counts. There are no further adjustable parameters. This allows to remove the aggregate effect of the "random" counts in the energy spectra [56–58].

In Fig. 8 we want to illustrate this by showing the 2D-energy spectrum obtained with $h\nu = 96$ eV. Figure 8(a) is the spectrum which contains only "true" counts which refers to the hatched area of Fig. 7. This is the result of removing the aggregate effect of "random" counts which we displayed in the manuscript. In Fig. 8(b) we display the spectrum which contains both "true" and "random" counts, this is the hatched plus dark-gray area in Fig. 7. The key point to notice is that the intensity distributions are hardly different. Furthermore, the intensity levels are very similar as evidenced by the same scale of the color coding. This implies that the contribution of "random" events is small in this investigation. This one can be evaluated numerically as presented in the dt curves in Fig. 9.

In Fig. 9(a) we show the curve which contains all measured events. We note a prominent peak and the width of the region of interest is indicated by the pair of vertical dashed lines. More importantly the peak height is much larger than the intensity level outside the peak region. This leads to a TR-ratio of 10.1 within the region of interest. In other words the contribution of "random" counts is an order of magnitude smaller than those from "true" counts. This large value is the reason why the 2D-energy plots in Fig. 8 can be hardly distinguished. Despite its small contribution we remove the "random" counts as explained above.

The focus of our work was the behavior of the diagonal intensity feature which is located within the dashed diagonal lines of Fig. 8. If we concentrate on these data we obtain the dt curve plotted in Fig. 9(b). Here the TR-ratio is larger and a value of 14.5 is obtained. The key mes-

sage is that our spectra are a very good representation of "true" events.

APPENDIX B: A PHENOMENOLOGICAL APECS MODEL

At high enough photon energy the core ionization channels are open and the direct double photoionization (DPE) contribution to the probability of generating photo-Auger electron pair can be neglected with respect to the resonant APECS one [59]. Following this hypothesis, Sawatzky computed the APECS cross section [56]. For energies well above the core ionization threshold and for lifetime of the core hole state large with respect to the electron-electron interaction time, the so-called two-step approximation holds. In this approximation only one intermediate state contributes to the transition matrix elements, that is the core hole state $|l_c\rangle$ generated in the photoemission process and the pair creation probability is proportional to

$$P(E_{\text{left}}, E_{\text{right}}) \propto \left| \frac{\langle f|V_c|l_c\rangle\langle l_c|D|i\rangle}{h\nu - BE_{A^+} - e_P + i\Gamma} \right|^2 \times \delta\left(h\nu - E_B^{2e} - E_{\text{right}} - E_{\text{left}}\right), \quad \text{(B1)}$$

with a single neutral initial state $|i\rangle$, a single final double valence hole state $\langle f|$ and V_c as the electron-electron Coulomb interaction operator, D as the photon dipole interaction operator, $h\nu$ as the photon energy, E_B^{2e} as the binding energy of the final state, $\Gamma_{A^{++}}$ as the final state line width, and BE_{A^+} as the binding energy of the intermediate state that has Γ_{A^+} lifetime line width. The first bracket appearing in the modulus square is the probability amplitude of the Auger decay, while the second is the core photoionization amplitude. It is then appealing to build up a phenomenological model for the APECS 2D-energy distribution that reduces $P(E_{\text{left}} + E_{\text{right}})$ to the product of the probability distribution of the individual photo and Auger spectra [29] while imposing correlation between the energies of the electron pair according to the following energy balance:

$$E_{\text{left}} + E_{\text{right}} = h\nu - E_B^{2e}. \quad \text{(B2)}$$

The quantity $E_{\text{left}} + E_{\text{right}}$ is defined within an uncertainty determined by the uncertainty principle, $\Gamma_{A^{++}}$ on E_B^{2e}, i.e., by lifetime and width of the final double hole density of states. Upon validity of these conditions, Kostanovskyi *et al.* [29] have expressed the 2D-energy distribution in a more appropriate reference frame for the description of electron pairs covariant in energy. Namely, have assumed $P(E_{\text{left}}, E_{\text{right}})$ to be the product of two Lorentzians dependent on $(E_{\text{left}} + E_{\text{right}})$ and $(E_{\text{left}} - E_{\text{right}})$, thus obtaining the following function:

$$P(E_{\text{left}}, E_{\text{right}}) \propto \frac{\Gamma_{A^+}/2}{(\Gamma_{A^+}/2)^2 + [(E_{\text{left}} + E_{\text{right}}) - (\mu_p + \mu_A)]^2} \cdot \frac{\Gamma_{A^{++}}/2}{(\Gamma_{A^{++}}/2)^2 + [(E_{\text{left}} - E_{\text{right}}) - (\mu_p - \mu_A)]^2}, \quad \text{(B3)}$$

with $\mu_{p,A}$ the centroid and with Γ_{A^+} ($\Gamma_{A^{++}}$) the width of the photoelectron (Auger) electron peak. The resulting model can be applied to give experimental grounds to the evidence for the double core-hole decay that we claim in the manuscript.

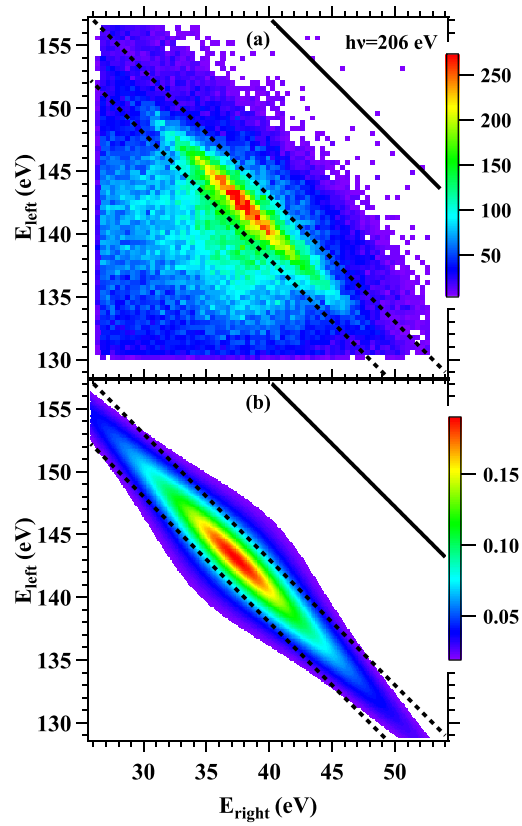

FIG. 10. Comparison of the experimental and simulated 2D-energy spectrum for $h\nu = 206$ eV. The data of panel (a) have been shown as Fig. 2(c) in the main text. The simulation exploring Lorentzian line shapes is plotted in panel (b). The solid diagonal lines refer to the position of $E_{\text{sum}}^{\max}$. The pairs of dashed lines indicate the energetic region used for the sharing curves.

The 2D-energy distribution measured at 206 eV [Fig. 2(c) in the main text] is ideally suited to apply the model being the photon energy large enough to clearly identify as photoelectrons the one measured by the left detector and as Auger those of the right detector. The experimental result is reported in Fig. 10 together with a simulation that assumes for the photoemission spectrum a Lorentzian fit function centered at 143.1 eV with 23 eV FWHM, and for the Auger spectrum a Lorentzian centered at 37.4 eV and equal width. $\Gamma_{A^{++}}$ is determined by the self-convolution of the $4d$ single particle density of states (DOS) reported in Fig. 3(a).

It is evident that the phenomenological simulation, even though rather crude, reproduces most of the relevant features of the experimental 2D-energy distribution. The width of the distribution along the $E_{\text{left}} + E_{\text{right}}$ direction for $E_{\text{left}} - E_{\text{right}} =$ const. is determined by the 2D DOS self-convolution, i.e., the two-hole DOS (about 4eV FWHM in this case), while the distribution along $-E_{\text{left}} - E_{\text{right}}$ for $E_{\text{left}} + E_{\text{right}} =$ const. reflects the breath of the energy share within the electron pair that is proportional to the energy spread of the core-hole intermediate state (23 eV in this case, that implies lower limit to the $4p^{-1}$ state lifetime of 30 as). The experimental counterpart of the distribution along $E_{\text{left}} - E_{\text{right}} =$ const. is approximated by a single Lorentzian function, as shown in Fig. 4(b) of the main text and therein discussed in detail. The model so

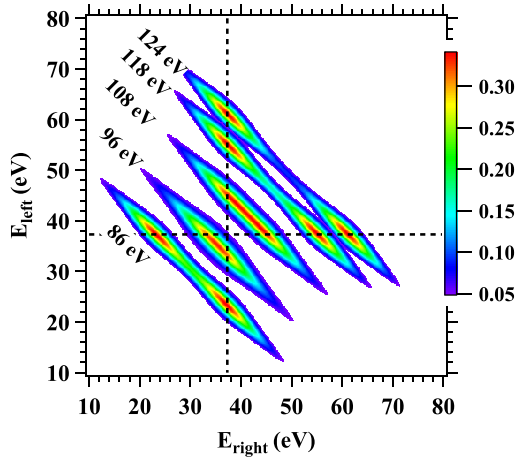

FIG. 11. Photon energy dependence of the 2D-energy distribution of the simulation. The horizontal and vertical dashed line represents the Auger kinetic energy.

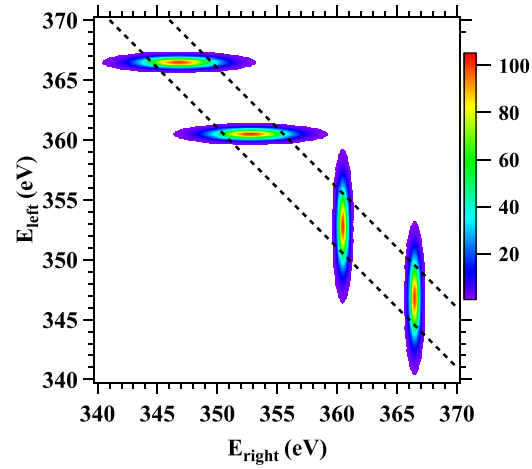

FIG. 12. Predicted Auger-photo electron emission from Ag upon excitation of the $3d$ level with $h\nu = 739$ eV. The pair of dashed diagonal lines define a E_{sum} range which on the E_B^{2e} scale is identical to those in Fig. 2.

far developed has been successfully applied to foresee the 2D-energy distributions at all other energies investigated in the experiment. The relevant results are shown in Fig. 11.

The energy distribution along $E_{\text{left}} + E_{\text{right}} = \text{const.}$, that represents the energy sharing within the electron pair energies, is always well represented by the sum of two Lorentzians identical to the one derived at 206 eV and set in mirror symmetric position with respect to the $E_{\text{left}} = E_{\text{right}}$ diagonal. This being the origin for the sum of two Lorentzian profiles compared with the experiments in Figs. 4 and 5 of the main text. We have added to this figure a horizontal and vertical dashed line which indicate the kinetic energy of the Auger electron. This helps to identify the center of the intensity pockets. Via the photon energy we can adjust the energy separation of the photoelectron-Auger pockets. Starting at $h\nu = 124$ eV these are well separated. Upon reducing the photon energy they come closer and at $h\nu = 108$ eV one can no longer identify two pockets, but observes a broad range of high intensity. This broad region reduces its extension for $h\nu = 96$ eV. A further reduction of the photon energy to 86 eV leads to the emergence of two well separated pockets. The intersection of the two dashed lines is reached if the photon energy is set to 100 eV. Under these conditions the Auger and photoelectron have the same peak kinetic energy.

APPENDIX C: SPIN-ORBIT INTERACTION OF THE 4*p* LEVEL

One may wonder how the spin-orbit interaction of the $4p$ level enters in the description of the Auger-photo electron decay in the case of Ag(100). If one has a spin-orbit doublet then the differences in the binding energy lead to a "fast" and "slow" photoelectron, which have a "slow" and "fast" Auger electron counterpart. From the energy conservation (B2) the energy sum of a "fast"-"slow" electron pair is fixed. The energetic separation between a "fast" and "slow" photoelectron (Auger electron) is due to the strength of the spin-orbit interaction. The underlying assumption in this description is a two-step process in which the Auger electron emission proceeds after the photoelectron emission. These straightforward facts lead to a prediction on how a 2D-energy plot will look like. It will be a pair of horizontal and vertical lines which intercept the E_{sum} region. Following our previous work [29] we simulate this for the particular case of the Ag $3d$ emission and subsequent CVV Auger emission. Input for

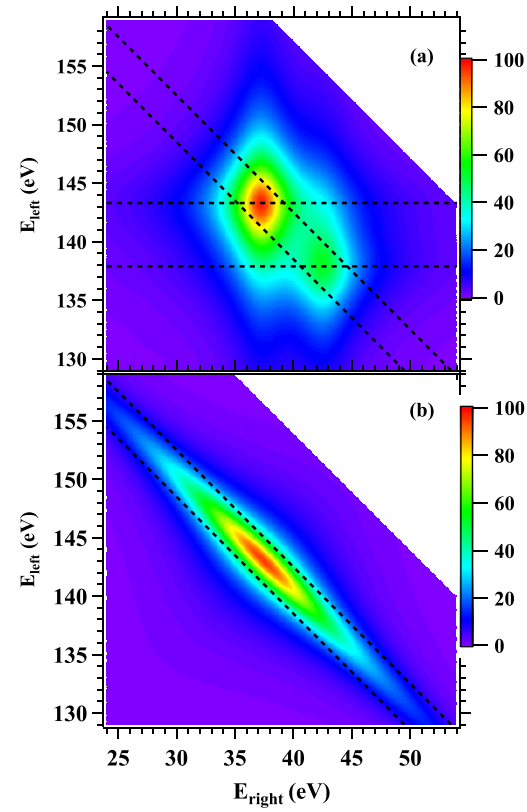

FIG. 13. We simulate the 2D-energy distribution for $h\nu = 206$ eV. Panel (a) is the result for the two-step process, while panel (b) shows the result for the one-step process. The pair of dashed diagonal lines define a E_{sum} range identical to those in Fig. 2(c).

the peak position is the XPS handbook [60]. The line width of the photoelectron is set to 0.7 eV, while the Auger width is 5 eV. These are not fit values, but are reasonably close to the experiment. If we select a photon energy of 739 eV Auger and photoelectron have similar energies. then we obtain Fig. 12. This result is close to our previous experimental observation [28].

We proceed by employing the same approach for the $4p$ derived Auger decay. As far as the $4p$ line shape is concerned we use the following input. The x-ray data booklet [50] lists the binding energy of the $4p$ levels at 63.7 and 58.3 eV. A line shape analysis of the $4p$ emission lines resulted in a Lorentzian width of 8.5 ($4p_{1/2}$) and 7.5 eV ($4p_{3/2}$) [61]. We used an average value of 8.0 eV for both lines. The kinetic energy of the Auger electrons are not readily available. However, we have shown that all our data have a sum energy peak at the same E_B^{2e} value. This information fixes the (two) Auger kinetic energies. The final input is the Auger electron width. We assume a width of 5 eV, which reflects the width of the self-convolution of the $4d$ valence band width. We also incorporated the different multiplicity by scaling the $4p_{1/2}$ part by a factor 0.5. This finally leads to Fig. 13(a), which we compare with the simulation employed in the main text. The photon energy was set to $h\nu = 206$ eV. The pair of dashed diagonal lines in both plots indicates the energy range where most of the (experimental) intensity was found. The pair of dashed horizontal lines in Fig. 13(a) indicate the energy positions of the $4p_{1/2}$ and $4p_{3/2}$ line. These lines intercept the region defined by the diagonal lines at different energy positions (or energy sharing). Energy conservation leads to white triangular regions in the upper right corner where no intensity exists. Comparing Figs. 13(a) and 13(b) we clearly see a different behavior, while the simulation in Fig. 13(b) has the intensity confined within the pair of red lines, this is not the case in Fig. 13(a). Since Fig. 13(b) reproduces the experimental findings, Fig. 13(a) does not.

[1] T. A. Carlson and M. O. Krause, Experimental evidence for double electron emission in an Auger process, Phys. Rev. Lett. **14**, 390 (1965).

[2] Y. Hikosaka, P. Lablanquie, F. Penent, P. Selles, T. Kaneyasu, E. Shigemasa, J. H. D. Eland, and K. Ito, Probing the mechanism of simultaneous two-electron emission on core-hole decay, Phys. Rev. A **80**, 031404(R) (2009).

[3] J. H. D. Eland, M. Tashiro, P. Linusson, M. Ehara, K. Ueda, and R. Feifel, Double core hole creation and subsequent Auger decay in NH_3 and CH_4 Molecules, Phys. Rev. Lett. **105**, 213005 (2010).

[4] M. Žitnik, R. Puttner, G. Goldsztejn, K. Bucar, M. Kavcic, A. Mihelic, T. Marchenko, R. Guillemin, L. Journel, O. Travnikova, D. Ceolin, M.N. Piancastelli, and M. Simon, Two-to-one Auger decay of a double L vacancy in argon, Phys. Rev. A **93**, 021401(R) (2016).

[5] Y. Hikosaka, P. Lablanquie, F. Penent, T. Kaneyasu, E. Shigemasa, R. Feifel, J. H. D. Eland, and K. Ito, Energy correlation of the three electrons emitted during the triple photoionization of Ar, Phys. Rev. Lett. **102**, 013002 (2009).

[6] P. Lablanquie, F. Penent, J. Palaudoux, L. Andric, P. Selles, S. Carniato, K. Bucar, M. Zitnik, M. Huttula, J. H. D. Eland *et al.*, Properties of hollow molecules probed by single-photon double ionization, Phys. Rev. Lett. **106**, 063003 (2011).

[7] E. P. Månsson, D. Guénot, C. L. Arnold, D. Kroon, S. Kasper, J. M. Dahlström, E. Lindroth, A. S. Kheifets, A. L'Huillier, S. L. Sorensen *et al.*, Double ionization probed on the attosecond timescale, Nat. Phys. **10**, 207 (2014).

[8] M. Schultze, M. Fiess, N. Karpowicz, J. Gagnon, M. Korbman, M. Hofstetter, S. Neppl, A. L. Cavalieri, Y. Komninos, Th. Mercouri *et al.*, Delay in photoemission, Science **328**, 1658 (2010).

[9] M. Drescher, M. Hentschel, R. Kienberger, M. Uiberacker, V. Yakovlev, A. Scrinzi, T. Westerwalbesloh, U. Kleineberg, U. Heinzmann, and F. Krausz, Time-resolved atomic inner-shell spectroscopy, Nature (London) **419**, 803 (2002).

[10] L. J. Frasinski, V. Zhaunerchyk, M. Mucke, R. J. Squibb, M. Siano, J. H. D. Eland, P. Linusson, P. v. d.M eulen, P. Salen, R. D. Thomas *et al.*, Dynamics of hollow atom formation in intense x-ray pulses probed by partial covariance mapping, Phys. Rev. Lett. **111**, 073002 (2013).

[11] C. Guillot, Y. Ballu, J. Paigné, J. Lecante, K. P. Jain, P. Thiry, R. Pinchaux, Y. Pétroff, and L. M. Falicov, Resonant photoemission in nickel metal, Phys. Rev. Lett. **39**, 1632 (1977).

[12] M. Iwan, F. J. Himpsel, and D. E. Eastman, Two-electron resonance at the $3p$ threshold of Cu and Ni, Phys. Rev. Lett. **43**, 1829 (1979).

[13] S. Hüfner, *Photoelectron Spectroscopy* (Springer, Berlin, 2003).

[14] W. Wurth and D. Menzel, Ultrafast electron dynamics at surfaces probed by resonant Auger spectroscopy, Chem. Phys. **251**, 141 (2000).

[15] I. Coulthard, T. K. Sham, Y. F. Hu, S. J. Naftel, P. S. Kim, and J. W. Freeland, Threshold behavior of the Cu$L_3M_{4,5}M_{4,5}$ Auger effect of Cu metal at the L_3 edge, Phys. Rev. B **64**, 115101 (2001).

[16] A. Föhlisch, P. Feulner, F. Hennies, A. Fink, D. Menzel, D. Sanchez-Portal, P. M. Echenique, and W. Wurth, Direct observation of electron dynamics in the attosecond domain, Nature (London) **436**, 373 (2005).

[17] F. O. Schumann, R. S. Dhaka, G. A. van Riessen, Z. Wei, and J. Kirschner, Surface state and resonance effects in electron pair emission from Cu(111), Phys. Rev. B **84**, 125106 (2011).

[18] G. A. van Riessen, F. O. Schumann, M. Birke, C. Winkler, and J. Kirschner, Correlated positron-electron emission from LiF (100), J. Phys.: Conf. Ser. **185**, 012051 (2009).

[19] G. A. van Riessen, Z. Wei, R. S. Dhaka, C. Winkler, F. O. Schumann, and J. Kirschner, Direct and core-resonant double photoemission from Cu(001), J. Phys.: Condens. Matter **22**, 092201 (2010).

[20] G. A. van Riessen, F. O. Schumann, M. Birke, C. Winkler, and J. Kirschner, Correlated positron-electron emission from surfaces, J. Phys.: Condens. Matter **20**, 442001 (2008).

[21] F. O. Schumann, G. Di Fillippo, Z. Wei, and G. Stefani, Chirality in double photoemission from a Cu(100) surface, J. Vac. Sci. Technol. A **40**, 043204 (2022).

[22] S. M. Thurgate, Coincidence measurements in the electron spectroscopies: Surface studies, Surf. Interface Anal. **20**, 627 (1993).

[23] W. Bothe and H. Geiger, Über das Wesen des Comptoneffekts; ein experimenteller Beitrag zur Theorie der Strahlung, Z. Phys. A **32**, 639 (1925).

[24] I. E. McCarthy and E. Weigold, (e, 2e) spectroscopy, Phys. Rep. **27**, 275 (1976).

[25] K. J. S. Sawhney, F. Senf, M. Scheer, F. Schäfers, J. Bahrdt, A. Gaupp, and W. Gudat, A novel undulator-based PGM beamline for circularly polarised synchrotron radiation at BESSY II, Nucl. Instrum. Methods Phys. Res., Sect. A **390**, 395 (1997).

[26] M. R. Weiss, R. Follath, K. J. S. Sawhney, F. Senf, J. Bahrdt, W. Frentrup, A. Gaupp, S. Sasaki, M. Scheer, H.-C. Mertins *et al.*, The elliptically polarized undulator beamlines at BESSY II, Nucl. Instrum. Methods Phys. Res., Sect. A **467-468**, 449 (2001).

[27] O. Gunnarsson and K. Schönhammer, Dynamical theory of Auger processes, Phys. Rev. B **22**, 3710 (1980).

[28] Z. Wei, F. O. Schumann, C. H. Li, L. Behnke, G. Di Filippo, G. Stefani, and J. Kirschner, Dynamic screening probed by core-resonant double photoemission from surfaces, Phys. Rev. Lett. **113**, 267603 (2014).

[29] I. Kostanovskiy, F. O. Schumann, Y. Aliaev, Z. Wei, and J. Kirschner, Core-resonant double photoemission from palladium films, J. Phys.: Condens. Matter **28**, 015601 (2016).

[30] G. Wendin, M. Ohno, and S. Lundqvist, New dynamical effects in the spectra of core holes, Solid State Commun. **19**, 165 (1976).

[31] G. Wendin, *Breakdown of the One Electron Pictures in Photoelectron Spectra* (Springer Verlag, Berlin, 1981).

[32] J. J. Lander, Auger peaks in the energy spectra of secondary electrons from various materials, Phys. Rev. **91**, 1382 (1953).

[33] M. Cini, Two hole resonances in the XVV Auger spectra of solids, Solid State Commun. **24**, 681 (1977).

[34] G. A. Sawatzky, Quasiatomic Auger spectra in narrow-band metals, Phys. Rev. Lett. **39**, 504 (1977).

[35] S. Hüfner, G. K. Wertheim, N. V. Smith, and M. M. Traum, XPS density of states of copper, silver, and nickel, Solid State Commun. **11**, 323 (1972).

[36] A. C. Parry-Jones, P. Weightman, and P. T. Andrews, The $M_{4,5}$ $N_{4,5}$ $N_{4,5}$ Auger spectra of Ag, Cd, In and Sn, J. Phys. C: Solid State Phys. **12**, 1587 (1979).

[37] D. A. Arena, R. A. Bartynski, R. A. Nayak, A. H. Weiss, and S. L. Hulbert, Line shape of the Ag $M_{4,5}$VV Auger spectra measured by Auger-photoelectron coincidence spectroscopy, Phys. Rev. B **63**, 155102 (2001).

[38] E. Jung, H. Q. Zhou, J. H. Kim, S. Starnes, R. Venkataraman, and A. H. Weiss, Background-free Auger line shape of Ag $N_{2,3}$VV measured with positron annihilation induced Auger electron spectroscopy, Appl. Surf. Sci. **116**, 318 (1997).

[39] F. O. Schumann, L. Behnke, C. H. Li, J. Kirschner, Y. Pavlyukh, and J. Berakdar, Electron pair emission from a highly correlated material, Phys. Rev. B **86**, 035131 (2012).

[40] A. Trützschler, M. Huth, C.-T. Chiang, R. Kamrla, F. O. Schumann, J. Kirschner, and W. Widdra, Band-resolved double photoemission spectroscopy on correlated valence electron pairs in metals, Phys. Rev. Lett. **118**, 136401 (2017).

[41] F. O. Schumann, Y. Aliaev, I. Kostanovskiy, and J. Kirschner, Double photoemission from Ag and Pd surfaces: Energy relations, Phys. Rev. B **101**, 115104 (2020).

[42] J. Viefhaus, S. Cvejanovic, B. Langer, T. Lischke, G. Prümper, D. Rolles, A. V. Golovin, A. N. Grum-Grzhimailo, N. M. Kabachnik, and U. Becker, Energy and angular distributions of electrons emitted by direct double Auger decay, Phys. Rev. Lett. **92**, 083001 (2004).

[43] J. Viefhaus, A. Grum-Grzhimailo, N. Kabachnik, and U. Becker, Electron-electron coincidence study of double Auger processes in atoms, J. Electron. Spectrosc. Relat. Phenom. **141**, 121 (2004).

[44] P. Lablanquie, L. Andric, J. Palaudoux, U. Becker, M. Braune, J. Viefhaus, J. Eland, and F. Penent, Multielectron spectroscopy: Auger decays of the argon 2p hole, J. Electron Spectrosc. Relat. Phenom. **156-158**, 51 (2007).

[45] L. Folkerts, J. Das, S. W. Bergsma, and R. Morgenstern, Three-electron Auger processes observed in collisions of bare ions on a metal surface, Phys. Lett. A **163**, 73 (1992).

[46] E. De Filippo, G. Lanzanò, H. Rothard, and C. Volant, Three-electron Auger process from beam-foil excited multiply charged ions, Phys. Rev. Lett. **100**, 233202 (2008).

[47] J. C. Slater, Atomic shielding constants, Phys. Rev. **36**, 57 (1930).

[48] M. Nakano, F. Penent, M. Tashiro, T. P. Grozdanov, M. Zitnik, S. Carniato, P. Selles, L. Andric, P. Lablanquie, J. Palaudoux *et al.*, Single photon K^{-2} and $K^{-1}K^{-1}$ double core ionization in $\mathbf{C}_2\mathbf{H}_{2n}$ ($n = 1-3$), CO, and $\mathbf{N}_2$ as a potential new tool for chemical analysis, Phys. Rev. Lett. **110**, 163001 (2013).

[49] J. J. Pireaux, S. Svensson, E. Basilier, P. A. Malmqvist, U. Gelius, R. Caudano, and K. Siegbahn, Core-electron relaxation energies and valence-band formation of linear alkanes studied in the gas phase by means of electron spectroscopy, Phys. Rev. A **14**, 2133 (1976).

[50] *X-Ray Data Booklet* (Center of X-ray Optics, Berkeley, CA).

[51] Gaussian16 (Gaussian Inc., Wallingford, CT, 2016).

[52] J. J. Yeh and I. Lindau, Atomic subshell photoionization cross sections and asymmetry parameters: $1 \leqslant Z \leqslant 103$, At. Data Nucl. Data Tables **32**, 1 (1985).

[53] S. L. Molodtsov, S. V. Halilov, V. D. P. Servedio, W. Schneider, S. Danzenbächer, J. J. Hinarejos, M. Richter, and C. Laubschat, Cooper minima in the photoemission spectra of solids, Phys. Rev. Lett. **85**, 4184 (2000).

[54] M. Völkel and W. Sandner, Optimisation of electron energy analysers for application in coincidence experiments, J. Phys. E **16**, 456 (1983).

[55] O. Kugeler, S. Marburger, and U. Hergenhahn, Calculation and measurement of the time-of-flight spread in a hemispherical electron energy analyzer, Rev. Sci. Instrum. **74**, 3955 (2003).

[56] G. A. Sawatzky, Auger photoelectron coincidence spectroscopy, in *Auger Electron Spectroscopy*, edited by R. P. Messmer and C. L. Briant (Academic Press, San Diego, CA, 1988).

[57] E. Jensen, R. A. Bartynski, S. L. Hulbert, and E. Johnson, Auger photoelectron coincidence spectroscopy using synchrotron radiation, Rev. Sci. Instrum. **63**, 3013 (1992).

[58] P. Calicchia, S. Lagomarsino, F. Scarinci, C. Martinelli, and V. Formoso, A study on background subtraction in Auger and photoelectron time coincidence spectroscopy using third generation synchrotron radiation source, Rev. Sci. Instrum. **70**, 3529 (1999).

[59] O. Gunnarsson and K. Schönhammer, Additional information in Auger-electron-photoelectron coincidence spectroscopy? Phys. Rev. Lett. **46**, 859 (1981).

[60] J. F. Moulder, W. F. Stickle, P. E. Sobol, and K. D. Bomben, *Handbook of X-ray Photoelectron Spectroscopy*, Physical Electronics Division (Perkin-Elmer Corporation, Eden Prairie, MN, 1992).

[61] M. H. Chen, B. Crasemann, L. I. Yin, T. Tsang, and I. Adler, Widths of atomic $4s$ and $4p$ vacancy states, $46 \leqslant Z \leqslant 50$, Phys. Rev. A **13**, 1435 (1976).